Journal of the Indian Chemical Society 103 (2026) 102601

Contents lists available at ScienceDirect

Journal of the Indian Chemical Society

journal homepage: www.journals.elsevier.com/journal-of-the-indian-chemical-society

Synthesis, binder optimization, and physicochemical characterization of activated carbon-zeolite-magnetite composites

Lydia Anggraini [a], Waqar Hussain [b,c,*], Kadek Dharmayudha Aryaputra [a], Syed Abdul Moiz Hashmi [b,c,d], Serene Lock Sow Mun [b,c], Hadiyawarman [e], Mahardika Fahrudin Rois [e]

[a] Department of Mechanical Engineering, President University, Jababeka Education Park, West Java, 17550, Indonesia
[b] Chemical Engineering Department, Universiti Teknologi PETRONAS, Bandar Seri Iskandar, 32610, Perak, Malaysia
[c] Centre for Sustainable Energy & Environmental Innovation (SEEI), University Teknologi PETRONAS, Seri Iskandar, Perak, 32610, Malaysia
[d] School of Engineering, STEM College, RMIT University, Melbourne, VIC, 3000, Australia
[e] National Research and Innovation Agency (BRIN), Indonesia

ARTICLE INFO

Keywords:
Magnetite composites
Activated carbon
Zeolite 13X
Physicochemical characterization
Binder effect

ABSTRACT

The development of multifunctional porous composites with tailored structural and surface properties is of significant interest for advanced material applications. In this work, activated carbon-zeolite-magnetite (AC-Z-Fe_3O_4) composites were synthesized via a one-pot hydrothermal method followed by carbonization, using citric acid or polyvinyl alcohol (PVA) as binders. Citric acid-assisted synthesis produced homogeneous composites with enhanced interfacial bonding and uniform magnetite distribution. Comprehensive physicochemical characterization was performed using scanning electron microscopy (SEM) coupled with energy-dispersive X-ray spectroscopy (EDS), X-ray diffraction (XRD), Fourier-transform infrared spectroscopy (FTIR), and nitrogen adsorption-desorption (BET) analyses. SEM-EDS confirmed the effective integration of activated carbon, zeolite, and magnetite phases, while XRD demonstrated retention of AC and magnetite crystallinity with partial preservation of the zeolite framework. FTIR indicated reduced surface hydrophilicity, and BET analysis revealed hierarchical micropore-mesopore structures with pore sizes below 20 Å. These structural and textural features establish the composites as robust, multifunctional materials with hierarchical porosity and tuneable surface properties. The systematic comparison of binder chemistry provides insights for designing integrated porous composites, establishing a foundation for future investigations into gas adsorption applications.

1. Introduction

The rapid increase in atmospheric CO_2 levels driven by fossil fuel–based energy production has raised significant environmental concerns [1]. Major emissions originate from coal- and gas-fired power plants, which has led to growing interest in post-combustion carbon capture technologies [2,3]. This approach is especially attractive due to its compatibility with existing industrial systems [4]. However, practical implementation remains challenging because of the low CO_2 partial pressure and the presence of nitrogen in flue gas, which demand materials with high surface area, optimized pore structure, strong chemical stability, and economic feasibility [5,6]. In this context, adsorption-based separation has gained attention as a viable alternative to conventional solvent-based methods, offering advantages such as lower energy requirements, reduced corrosion, and simpler operation [7]. Consequently, the development of advanced adsorbent materials has become a key focus, where performance is largely dictated by physicochemical characteristics, including surface area, pore volume, microporosity, and surface functional groups [8,9]. Consequently, extensive research has been devoted to the development of advanced porous materials such as activated carbons, zeolites, metal oxides, and composite adsorbents [10–12]. Activated carbon is widely studied owing to its high specific surface area, tunable pore structure, hydrophobic nature, and low production cost [12]. However, its relatively weak affinity toward CO_2 and limited selectivity in the presence of competing gases restrict its standalone applicability [13]. Zeolites, on the other hand, exhibit strong CO_2 affinity due to their well defined microporous frameworks and electrostatic interactions arising from

* Corresponding author. Chemical Engineering Department, Universiti Teknologi PETRONAS, Bandar Seri Iskandar, 32610, Perak, Malaysia.
E-mail address: waqar_24000524@utp.edu.my (W. Hussain).

https://doi.org/10.1016/j.jics.2026.102601
Received 15 January 2026; Received in revised form 6 April 2026; Accepted 9 April 2026
Available online 9 April 2026

framework cations [14]. Despite their excellent adsorption characteristics, zeolites often suffer from moisture sensitivity and diffusion limitations under practical operating conditions [15,16]. These limitations highlight the need for hybrid materials that can integrate the advantages of different adsorbent classes while mitigating their individual drawbacks [17,18]. Composite adsorbents have gained increasing attention as next-generation materials for gas separation applications due to their potential to exhibit synergistic structural and textural properties [13]. By combining porous carbons with crystalline inorganic frameworks, composite materials can offer hierarchical pore structures, improved mass transfer characteristics, and enhanced structural stability [19]. In this context, the incorporation of metal oxides into carbon-zeolite matrices represents an effective strategy to introduce additional functionality and structural tuning. Magnetite (Fe_3O_4) is a low-cost iron oxide with surface Lewis acidic (Fe^{2+}/Fe^{3+}) and Lewis basic (O^{2-}) sites capable of interacting with the quadrupole moment of CO_2 molecules [20] and also as a particularly attractive additive for composite adsorbent design due to its chemical stability, low toxicity, and magnetic properties. Beyond enabling facile magnetic separation and handling, magnetite nanoparticles can influence pore development, surface heterogeneity, and composite integrity when uniformly dispersed within porous matrices [21]. Several studies have demonstrated that magnetite-based composites exhibit improved structural robustness and tunable textural characteristics, making them promising candidates for adsorption-related applications. Nevertheless, systematic studies focusing on the structural integration of magnetite within activated carbon-zeolite systems and their resulting physicochemical properties remain limited [22–24].

In this work, a AC-Z-Fe_3O_4 composite adsorbent is synthesized and systematically characterized, with emphasis on its structural features and physicochemical properties arising from the material design and fabrication approach. The composite architecture integrates the high surface area and hydrophobicity of activated carbon, the crystalline microporosity of zeolite, and the structural reinforcement and magnetic functionality of magnetite. Comprehensive characterization using SEM, EDS, XRD, and nitrogen adsorption-desorption (BET) analysis is employed to elucidate morphology, phase integration, crystallinity, and pore structure. Rather than evaluating adsorption performance metrics, the scope of this study is deliberately focused on material design, interfacial compatibility, pore architecture, and structural integrity-critical prerequisites for any potential adsorption application. Specifically, this work systematically investigates the role of binder chemistry (citric acid vs. PVA) and magnetite incorporation on the structural and textural properties of AC-Z composites. By establishing a detailed understanding of how synthesis parameters affect composite formation, this study provides a foundational framework for future investigations into adsorption performance.

2. Materials and methods

2.1. Research framework

The overall research methodology followed a systematic framework consisting of material evaluation, composite synthesis, physicochemical characterization. The detailed research framework is illustrated in Fig. 1.

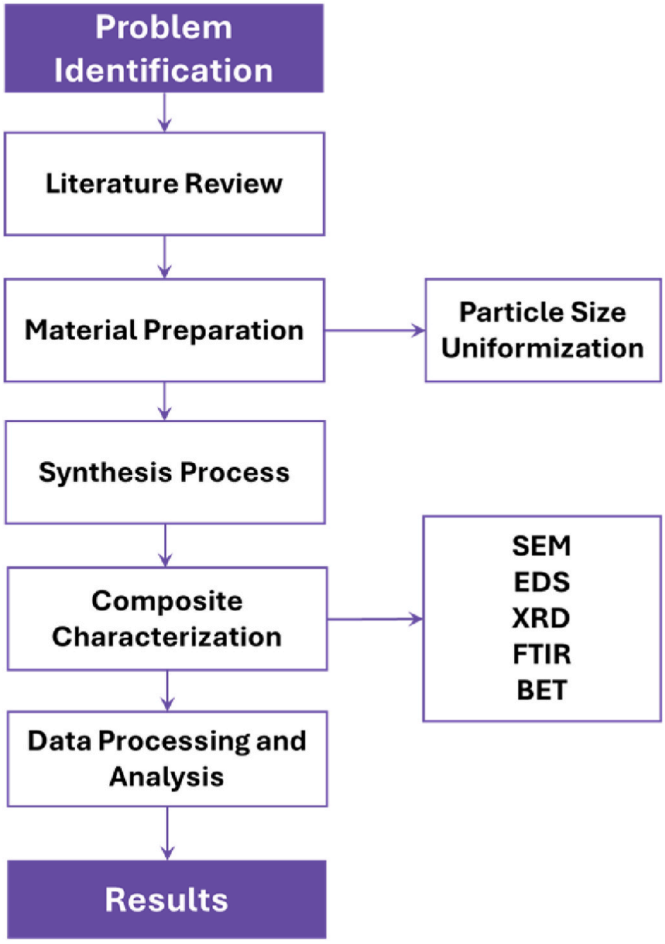

Fig. 1. Research framework flowchart.

2.2. Materials

AC, zeolite 13X, and magnetite (Fe_3O_4) were selected as the primary constituents for the fabrication of composite adsorbents due to their complementary physicochemical properties relevant to adsorption-based gas separation. The activated carbon was supplied by the Badan Riset dan Inovasi Nasional (BRIN), Indonesia, and was produced through high-temperature carbonization of chicken manure under an inert atmosphere to enhance porosity and remove volatile components. Prior to use, the activated carbon was ground and sieved to a particle size of 200 mesh to ensure uniform mixing with other components. Commercial zeolite 13X was procured from a local supplier (Henan Shengwell Environmental Protection Technology Co., Ltd.) and supplied in spherical granule form. The zeolite was mechanically crushed and sieved to 200 mesh to obtain a particle size comparable to that of the activated carbon. Analytical grade magnetite (Fe_3O_4) powder was purchased from Sigma-Aldrich and used without further purification to avoid compositional alteration. Citric acid monohydrate (analytical grade, Merck Chemicals) and PVA, analytical grade, Sigma-Aldrich) were employed as binder agents to improve interparticle adhesion and composite structural integrity. All aqueous solutions were prepared using deionized (DI) water to eliminate interference from dissolved ionic species.

2.3. Synthesis of AC-Z-Fe_3O_4 composite adsorbent

The composite adsorbents were synthesized via a one-pot hydrothermal route followed by thermal treatment under an inert atmosphere. This approach was selected to promote homogeneous dispersion of constituents while preserving the porous structure of the adsorbent matrix. A series of composite formulations were prepared to examine the influence of binder type and magnetite loading on the physicochemical properties of the resulting materials. The compositions of the synthesized samples are summarized in Table 1.

To prepare the base slurry, activated carbon (4.0 g) and zeolite 13X (4.0 g) were dispersed in 50 mL of deionized water and magnetically stirred for 20 min to ensure uniform suspension. For magnetite-containing composites, Fe_3O_4 powder was introduced into the AC-Z

Table 1
Composition of synthesized composite samples.

Sample ID	Primary Materials	Binder
KD-01	4g AC + 4g Zeolite 13X	Citric acid
KD-03	4g AC + 4g Zeolite 13X	-
KD-04	4g AC + 4g Zeolite 13X	PVA
KD-06	4g AC + 4g Zeolite 13X + 1g Fe_3O_4	Citric acid
KD-07	4g AC + 4g Zeolite 13X + 2g Fe_3O_4	Citric acid

slurry at loadings of 1.0 g or 2.0 g, followed by ultrasonication for 20 min to promote homogeneous dispersion and prevent particle agglomeration.

Binder solutions were prepared separately prior to addition. For citric acid binding, 2.0 g of citric acid monohydrate was dissolved in 20 mL of deionized water under magnetic stirring for 20 min. For PVA binding, 2.0 g of PVA was dissolved in 20 mL of deionized water at 100 °C until a clear and homogeneous solution was obtained. The respective binder solutions were then slowly added to the AC-Z or AC-Z-Fe_3O_4 slurry, followed by ultrasonication for an additional 20 min to ensure uniform coating and interparticle interaction.

The resulting homogeneous mixtures were transferred into Teflon-lined stainless-steel autoclaves and subjected to hydrothermal treatment at 110 °C for 3 h. After natural cooling to room temperature, the solid products were recovered by filtration and dried overnight under ambient conditions. The dried samples were subsequently carbonized in a tubular furnace under a nitrogen atmosphere using a controlled heating program to avoid structural collapse and preserve porosity. After carbonization, the composite materials were ground and sieved to 200 mesh to obtain uniform powders suitable for physicochemical characterization. A schematic representation of the synthesis procedure is shown in Fig. 2.

2.4. Physicochemical characterization

The morphology and surface characteristics of the synthesized composite adsorbents were examined using SEM to assess particle size distribution, surface roughness, and structural integration among composite constituents. Elemental composition and spatial distribution were analyzed using EDS coupled with SEM. The crystalline structure and phase composition of the materials were investigated using XRD. Diffraction patterns were recorded over an appropriate 2θ range, and characteristic reflections were used to identify crystalline phases corresponding to magnetite and zeolite, as well as to assess structural stability following composite formation. Surface functional groups and chemical interactions between composite components were analyzed using Fourier-transform infrared spectroscopy (FTIR). Spectra were recorded in the mid-infrared region to identify functional groups originating from activated carbon, zeolite frameworks, and binder agents. Textural properties, including specific surface area, pore volume, and pore size distribution, were determined using nitrogen adsorption-desorption measurements conducted at 77 K. Prior to analysis, samples were degassed under vacuum to remove adsorbed moisture and gases. The Brunauer-Emmett-Teller (BET) method was employed to calculate specific surface area, while pore size distribution and total pore volume were derived from adsorption data using appropriate models.

3. Results and discussion

3.1. Physicochemical characterization of AC-Z-Fe_3O_4 composites

The synthesized AC-Z-Fe_3O_4 composites were comprehensively characterized to evaluate structural integrity, morphological features, chemical composition, and textural properties. SEM, EDS, XRD, FTIR, and BET analyses were employed to understand how the synthesis strategy affects material integration and properties relevant to post-combustion CO_2 capture.

3.1.1. Morphology and elemental distribution (SEM-EDS)

SEM analysis was conducted to investigate the surface morphology and microstructural integration of the composite constituents. Fig. 3(a) presents the SEM micrograph of sample KD-01, synthesized using citric acid as a binder, at a magnification of 1000 × . The composite exhibits irregularly shaped particles with sizes ranging from approximately 10 to 30 μm. Two distinct morphological domains are evident: darker, rounded regions corresponding to activated carbon and brighter, angular regions attributed to zeolite particles, as confirmed by EDS analysis.

EDS spectra obtained from representative regions reveal that the red highlighted (Fig. 3(c)) region contains a high carbon content (~87 wt %), whereas the green highlighted region (Fig. 3(b)) contains measurable silicon (~3 wt%) and aluminum, confirming the coexistence of activated carbon and zeolite phases within the composite. Importantly, the close interfacial contact between these domains indicates effective particle binding and successful composite formation, highlighting the role of citric acid in promoting interparticle cohesion during hydrothermal synthesis.

In contrast, the SEM-EDS results for sample KD-03, synthesized without a binder (Fig. 4), reveal a markedly different morphology. Although the elemental composition confirms the presence of activated carbon (~89 wt% C) (green circle; Fig. 4(b)) and zeolite (~8 wt% Si and ~5 wt% Al rich regions) (red square; Fig. 4(c)), the two phases appear largely segregated, with minimal interfacial interaction.

Sample KD-04, prepared using PVA as a binder, exhibits a morphology similar to KD-03, characterized by dispersed fine zeolite particles with limited adhesion to the AC matrix (Fig. 5(a)). While localized regions (blue marked area) show partial zeolite coating on AC surfaces, these interactions are sparse compared to KD-01. EDS analysis further supports this observation: the bonded region (green circle; Fig. 5 (c)) contains ~83 wt% carbon with trace Si and Al, while the unbonded region (red circle; Fig. 5(b)) contains ~34 wt% carbon, 7 wt% Al, and 9

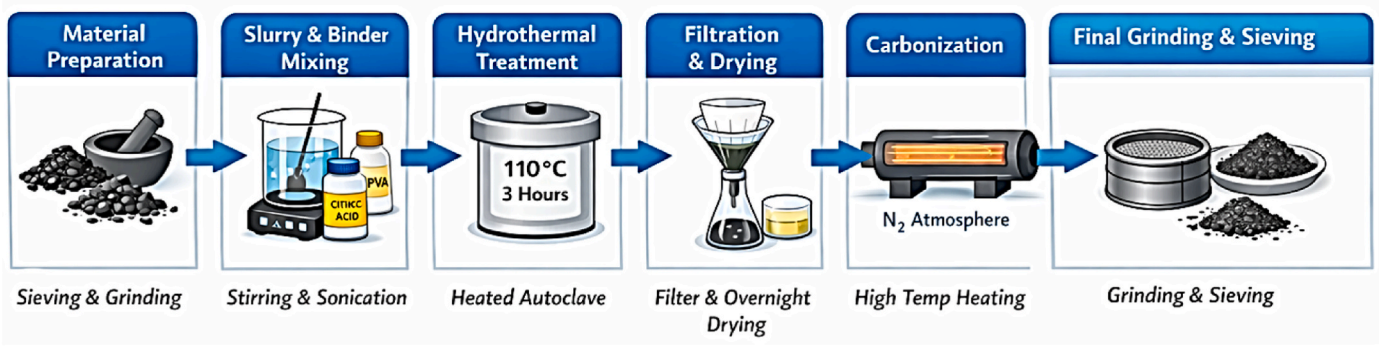

Fig. 2. Composite synthesis process flow.

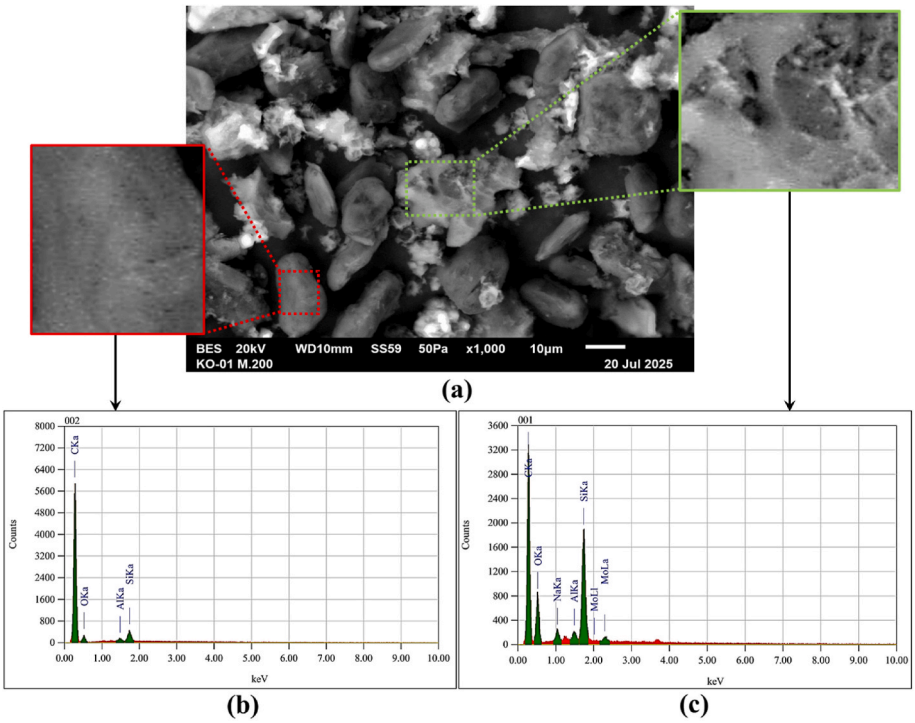

Fig. 3. KD-01 image of (a) SEM in ×1000 magnification (b) EDS red highlighted region (c) EDS green highlighted region.

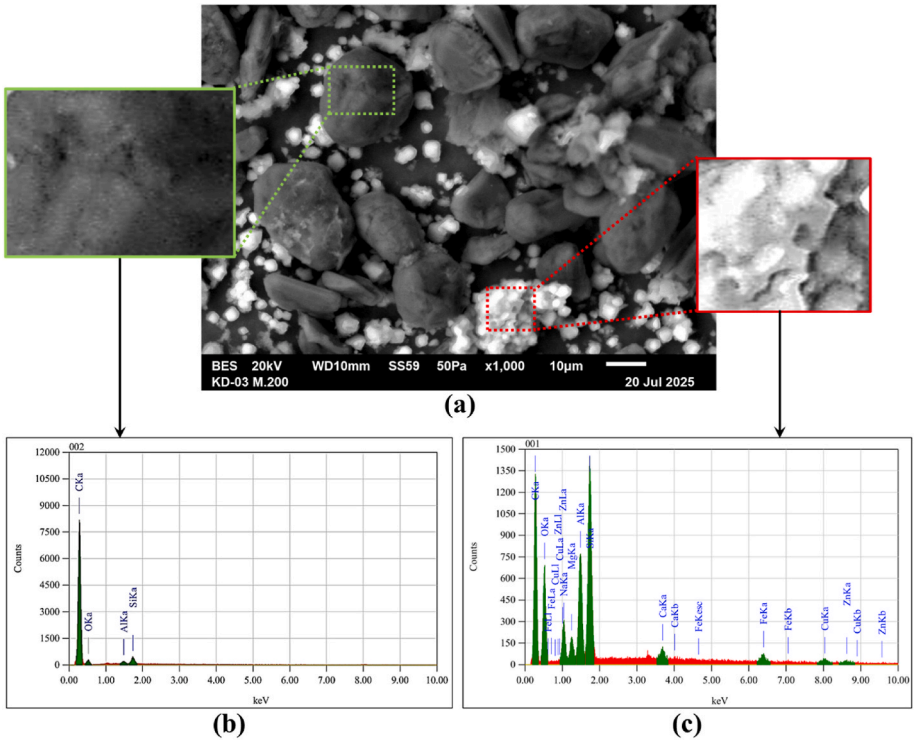

Fig. 4. KD-03 image of (a) SEM in ×1000 magnification (b) EDS green highlighted region (c) EDS red highlighted region.

wt% Si.

SEM-EDS analysis of magnetite-containing samples KD-06 and KD-07 (Figs. 6 and 7) confirms successful incorporation of Fe_3O_4 into the composite structure. Fe is clearly detected in the Fe-rich regions, with Fe contents of approximately 14 wt% for KD-06 and 36 wt% for KD-07, consistent with the intended magnetite loadings. Morphologically, both samples exhibit improved phase integration and reduced segregation of zeolite particles, closely resembling the microstructure of KD-01.

SEM analysis (Figs. 3–7) revealed clear differences in phase integration. KD-01 (citric acid) exhibited intimate contact between AC and zeolite domains (Fig. 3(a)), while KD-03 (binder-free) showed pronounced phase segregation (Fig. 4(a)). KD-04 (PVA) demonstrated intermediate adhesion (Fig. 5(a)). Magnetite-containing samples (KD-06,

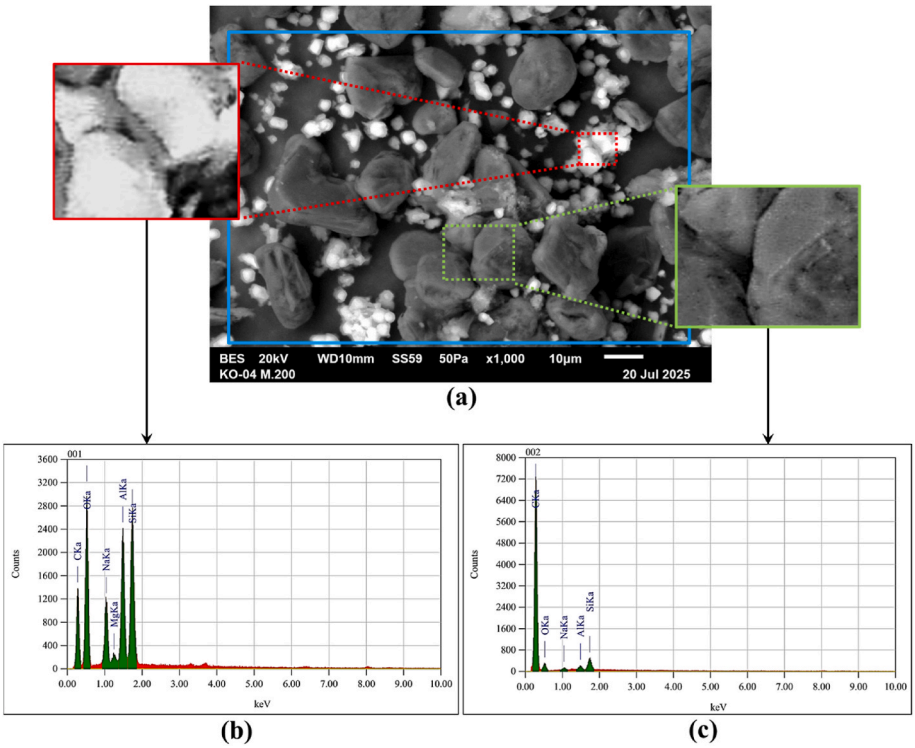

Fig. 5. KD-04 image of (a) SEM in ×1000 magnification (b) EDS red highlighted region (c) EDS green highlighted region.

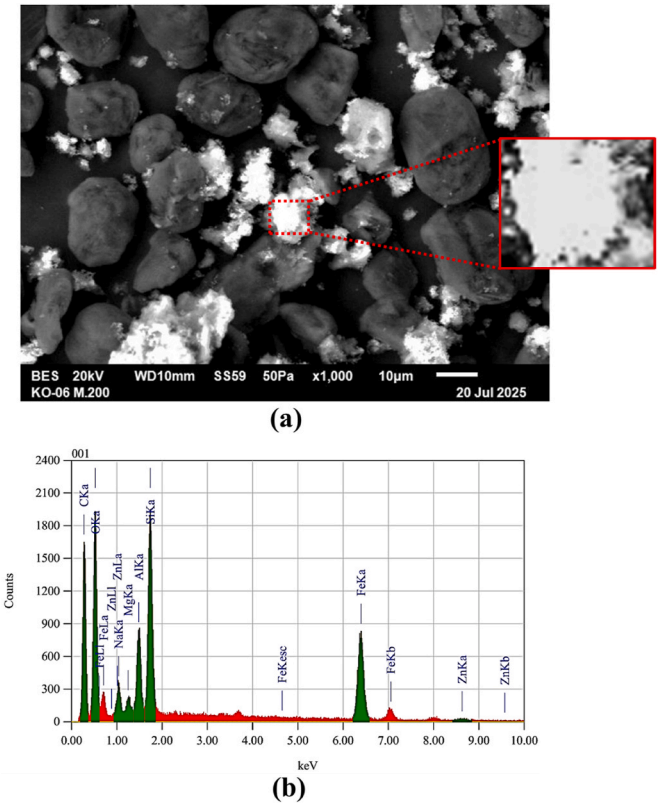

Fig. 6. KD-06 image of (a) SEM in ×1000 magnification (b) EDS red highlighted region.

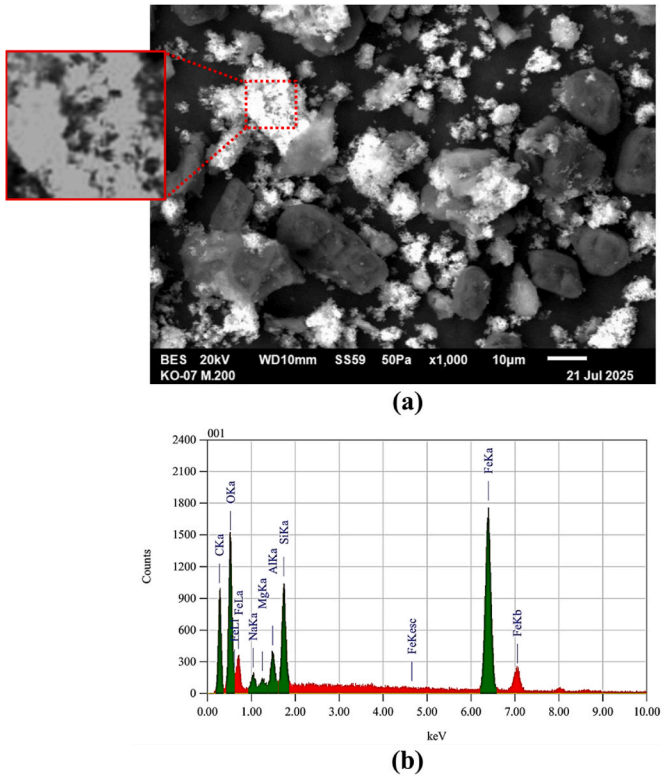

Fig. 7. KD-07 image of (a) SEM in ×1000 magnification (b) EDS red highlighted region.

KD-07) maintained the well-integrated morphology characteristic of citric acid-bound composites, with EDS confirming homogeneous Fe distribution (Figs. 6 and 7).

To further verify the magnetic functionality of the composites, a digital photograph demonstrating their response to an external magnetic field is presented in Fig. 8. The clear attraction of the composite particles toward the magnet confirms the successful incorporation of magnetite

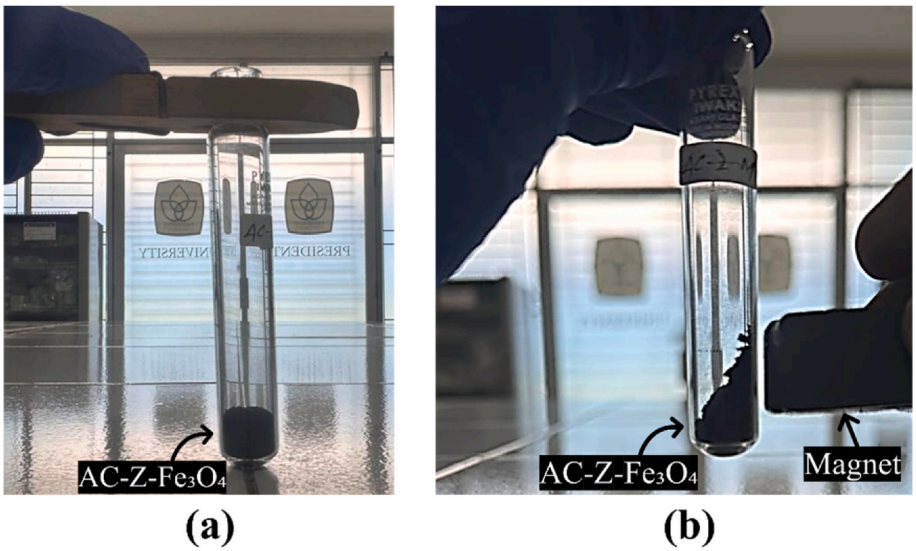

Fig. 8. Magnetic response of AC-Z-Fe_3O_4 composite, (a) Uniform dispersion of particles prior to magnetic field application, (b) Rapid migration and accumulation of particles toward an external magnet, confirming the successful incorporation of magnetite and magnetic separability of the composite.

and the resulting magnetic behavior.

Overall, SEM-EDS analysis demonstrates that citric acid plays a crucial role in achieving homogeneous composite formation, while controlled magnetite incorporation does not compromise structural integrity. The observed microstructural integration is a key prerequisite for achieving favorable adsorption-relevant properties.

3.1.2. XRD analysis

XRD analysis was performed to identify crystalline phases and assess structural preservation following composite synthesis. Fig. 8 presents the diffraction patterns of the primary materials and representative composite samples.

Activated carbon exhibits a broad diffraction feature centered around 26°, characteristic of turbostratic carbon structures. This feature is retained in all composite samples, indicating that the carbonaceous framework remains structurally stable during synthesis. Pristine zeolite 13X displays multiple sharp diffraction peaks at low angles (approximately 7°, 9°, 12°, and 16°), corresponding to its ordered aluminosilicate framework. In the composite samples, the intensity of these zeolite-related reflections is significantly reduced. This attenuation may arise from multiple factors, including physical dilution within the composite matrix (zeolite comprises only half of the solid components), partial masking by amorphous carbon and magnetite phases, and possible structural degradation of the zeolite framework during hydrothermal treatment or carbonization. Zeolite 13X is known to be sensitive to hydrothermal conditions, and framework collapse or dealumination can occur under elevated temperature and pressure in aqueous environments. The hydrothermal synthesis step (110 °C for 3 h) may have induced partial structural damage, particularly at the external surfaces of zeolite crystallites, and the subsequent carbonization step could further affect zeolite crystallinity.

However, several observations suggest that some zeolite structural elements remain intact. FTIR analysis (Fig. 10) confirms the preservation of characteristic Si–O–Al stretching vibrations in the 900-1200 cm^{-1} region for all composites, indicating that the fundamental aluminosilicate framework is retained. EDS analysis (Figs. 3–7) consistently detected silicon and aluminum in the composite matrices, with Al/Si ratios approximating that of pristine zeolite. Furthermore, residual low-intensity peaks corresponding to zeolite reflections are still discernible in the composite patterns, particularly in KD-01, suggesting partial rather than complete framework destruction.

Magnetite-containing composites KD-06 and KD-07 exhibit distinct diffraction peaks at approximately 30°, 35°, 43°, 54°, 57°, and 64°, corresponding to the characteristic reflections of Fe_3O_4. The presence and sharpness of these peaks confirm successful incorporation of magnetite without phase transformation or significant crystallinity loss during synthesis. Notably, no additional peaks corresponding to iron-silicate or iron-aluminate phases were detected, suggesting that magnetite remains as a discrete phase without extensive chemical reaction with the zeolite framework. This phase separation is beneficial for maintaining the individual functionalities of each component. The coexistence of the amorphous carbon feature, residual zeolite reflections, and sharp magnetite peaks highlights the multiphase nature of the composite adsorbents.

3.1.3. Fourier-transform infrared spectroscopy (F-TIR) analysis

FTIR spectroscopy was employed to analyze surface functional groups and chemical interactions among composite constituents. As shown in Fig. 10, all samples exhibit a broad absorption band around 3400 cm^{-1}, associated with O–H stretching vibrations from adsorbed water and surface hydroxyl groups. Pristine zeolite shows the most intense hydroxyl absorption, reflecting its hydrophilic nature, while activated carbon exhibits relatively weak absorption in this region.

The composite samples display notably reduced O–H band intensity compared to zeolite, indicating partial surface modification toward lower hydrophilicity. This behavior is beneficial for post-combustion CO_2 capture, as excessive hydrophilicity can adversely affect adsorption performance under humid flue gas conditions. Additionally, the characteristic Si–O–Al stretching vibrations in the 900–1200 cm^{-1} region are preserved in all composite samples, confirming the structural integrity of the zeolite framework after composite formation.

While the presence of magnetite introduces potential Lewis acid-base sites (Fe^{2+}/Fe^{3+}) that could theoretically interact with CO_2, direct evidence for such interactions requires techniques such as CO_2-temperature programmed desorption (CO_2-TPD) or in situ spectroscopy. In the current study, the role of magnetite is primarily structural (influencing pore development) and functional (providing magnetic separability), with chemical interactions with adsorbates remaining to be confirmed.

3.1.4. Textural properties

Nitrogen adsorption-desorption measurements were conducted at 77 K to evaluate the textural properties of the synthesized composites. The specific surface area was calculated using the BET method, while total pore volume was determined from the amount adsorbed at $P/P_0 \approx$

0.99. Micropore volume was obtained via t-plot analysis. A summary of the textural parameters for all samples is presented in Table 2.

The textural properties varied significantly with binder type, consistent with SEM observations of phase integration. KD-01 (citric acid binder) exhibited the highest surface area (550 m^2/g) and pore volumes (total: 0.32 cm^3/g; micropore: 0.21 cm^3/g), correlating with the homogeneous phase distribution seen in Fig. 3 where intimate AC-Z contact facilitates an interconnected pore network. Carbonization of citric acid may also contribute additional microporous carbon [23]. In contrast, KD-03 (binder-free) showed the lowest values (400 m^2/g; 0.24 cm^3/g; 0.13 cm^3/g), directly reflecting the phase-segregated morphology in Fig. 4 where poor interfacial contact limits pore development. KD-04 (PVA binder) demonstrated intermediate properties (430 m^2/g; 0.26 cm^3/g; 0.15 cm^3/g), consistent with Fig. 5 showing only partial particle adhesion, confirming that PVA is less effective than citric acid for promoting optimal porosity.

Magnetite-containing composites exhibited systematic textural changes. KD-06 (1 g Fe_3O_4) showed surface area of 500 m^2/g and total pore volume of 0.28 cm^3/g, slightly lower than KD-01 due to dilution by low surface area magnetite (typical Fe_3O_4 BET: ~95 m^2/g [24]). However, its micropore volume (0.19 cm^3/g) represents approximately 68% of total pore volume, higher than KD-01 (~65%), suggesting magnetite influences pore development beyond simple dilution. KD-07 (2 g Fe_3O_4) showed further reduction in surface area (450 m^2/g) and total pore volume (0.26 cm^3/g), yet maintained a high micropore fraction (~65%). XRD analysis (Fig. 9) confirms magnetite crystallinity is preserved in both composites, indicating Fe_3O_4 particles remain structurally intact and capable of influencing pore architecture.

The observed variation in BET surface area and pore volume from the raw materials to the final composites can be attributed to the combined effects of pore blocking, pore modification, and phase dilution during composite formation. In particular, the incorporation of magnetite nanoparticles plays a critical role in altering the pore architecture. Due to their nanoscale size, Fe_3O_4 particles can become localized both on the external surface and within the internal pore channels of activated carbon and zeolite. Partial occupation of micropores by magnetite may reduce the accessible surface area by limiting nitrogen adsorption, a phenomenon commonly referred to as pore blocking. Simultaneously, magnetite particles may line the internal walls of larger pores, effectively narrowing pore diameters and contributing to the observed shift toward smaller pore sizes. This dual effect explains the reduction in overall surface area with increasing magnetite loading, while maintaining or even enhancing the fraction of microporosity. In addition, the inherently low surface area of magnetite compared to activated carbon further contributes to the apparent decrease in BET surface area through a dilution effect. Therefore, the final textural properties of the composites result from a balance between structural integration, pore accessibility, and nanoparticle distribution within the porous matrix.

Table 2
Textural properties of synthesized composite adsorbents.

Sample	Composition	Binder	BET surface area (m^2/g)	Total pore volume (cm^3/g)	Micropore volume (cm^3/g)
KD-01	AC (4g) + Zeolite (4g)	Citric Acid	550	0.32	0.21
KD-03	AC (4g) + Zeolite (4g)	None	400	0.24	0.13
KD-04	AC (4g) + Zeolite (4g)	PVA	430	0.26	0.15
KD-06	AC (4g) + Zeolite (4g) + Fe_3O_4 (1g)	Citric Acid	500	0.28	0.19
KD-07	AC (4g) + Zeolite (4g) + Fe_3O_4 (2g)	Citric Acid	450	0.26	0.17

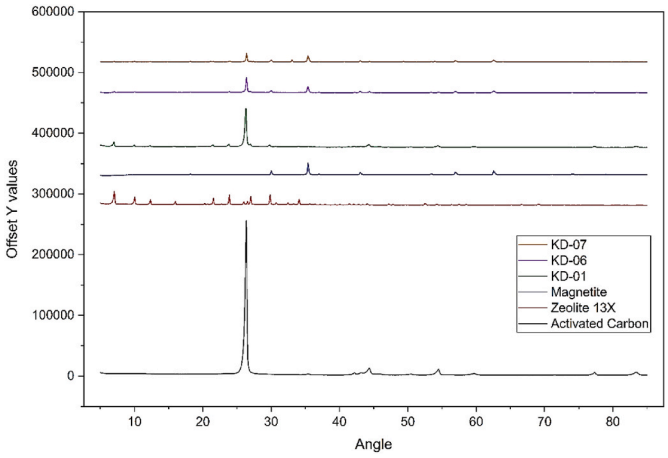

Fig. 9. XRD result of primary material with KD specimen.

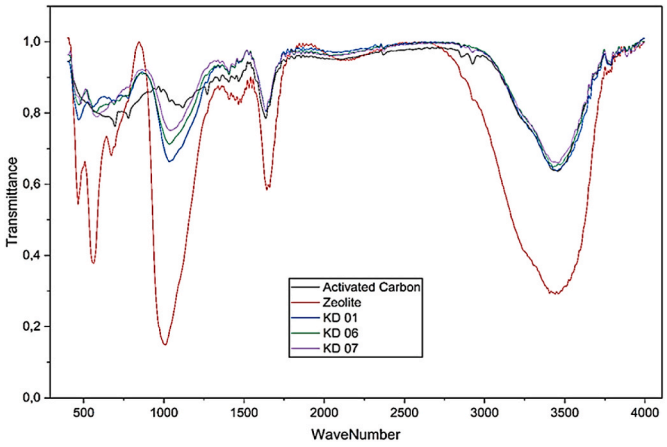

Fig. 10. FTIR Analysis comparison with KD specimens with Zeolite and AC.

Pore size distribution analysis (Fig. 11) provides additional insight into the effect of magnetite incorporation. Although the average pore diameters reported in Table 2 are larger than the kinetic diameter of CO_2 (3.3 Å [25]), the pore size distributions reveal that a substantial fraction of pores lies below 20 Å, which is particularly relevant for gas confinement. All citric acid-bound composites (KD-01, KD-06, KD-07) exhibit hierarchical porosity combining micropores (<20 Å) with small mesopores. Notably, magnetite-containing samples (KD-06 and KD-07) display a higher proportion of pores in the sub-20 Å range compared to KD-01 (Fig. 10), confirming that magnetite incorporation promotes narrow micropore development, consistent with trends reported for zeolite-carbon composite systems in the literature. This pore refinement with increasing magnetite content, where nanoparticles may occupy or line larger pores, effectively narrowing pore channels has been reported in similar magnetic composite systems [21,24].

The importance of micropore structure, particularly in composite systems, has been widely reported in the literature. For instance, Panek et al. [26] demonstrated that carbon-zeolite composites derived from fly ash exhibit enhanced adsorption performance due to the development of well defined microporous structures and improved surface heterogeneity. Similarly, Zhou et al. [27] reported that core-shell carbon-zeolite composites synthesized from biomass-derived precursors exhibit improved pore architecture and surface accessibility, which are closely linked to enhanced adsorption and catalytic performance. In addition, Bandura et al. [28] verified that zeolite-carbon composites prepared from high carbon fly ash possess tailored microporous networks that significantly influence adsorption behavior toward organic compounds.

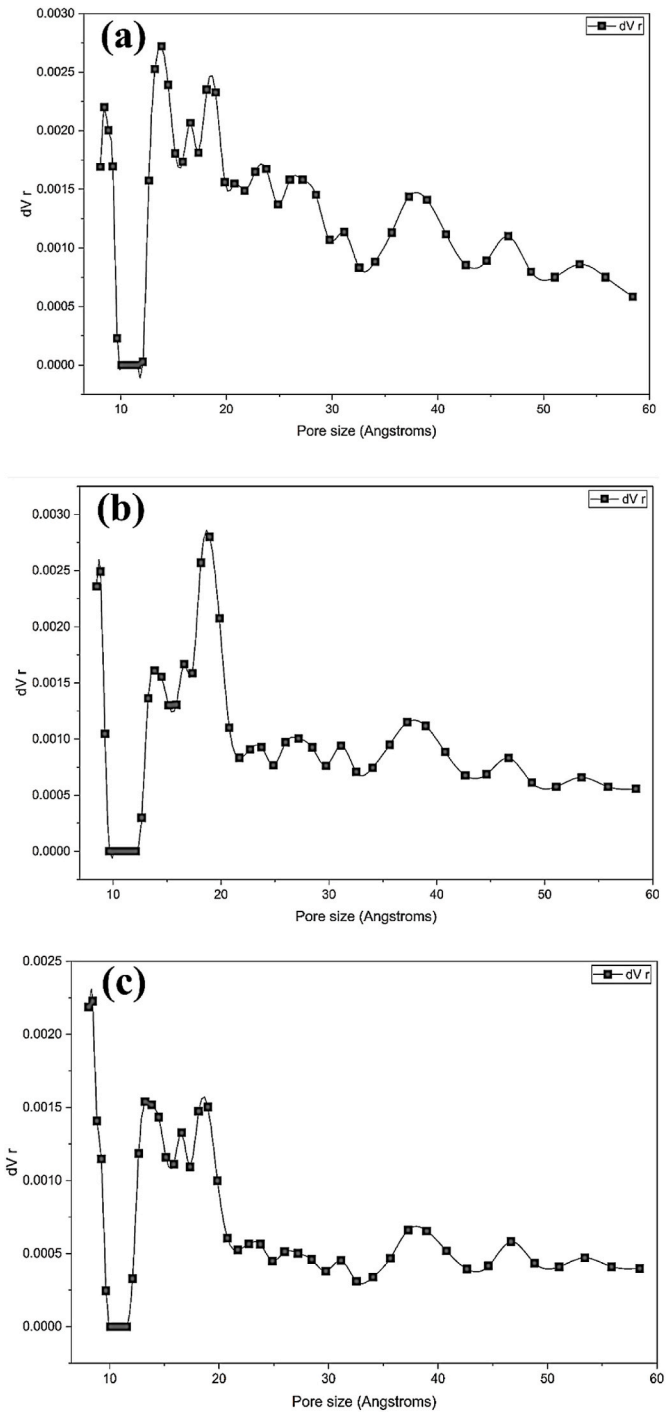

Fig. 11. Pore size distribution of (a) KD-01, (b) KD-06, and (c) KD-07.

These studies collectively highlight that the formation and modification of micropores in composite materials are strongly dependent on synthesis strategy and component integration. In the present work, the observed increase in the fraction of narrow pores (<20 Å), particularly in magnetite-containing samples, is consistent with these findings and further supports the role of composite design in tuning pore structure.

The coexistence of micropores (providing adsorption sites) and mesopores (facilitating gas transport) is advantageous for adsorption applications. FTIR analysis (Fig. 10) complements these findings by showing reduced surface hydrophilicity in all composites compared to pristine zeolite, which may benefit adsorption under humid conditions.

3.1.5. *Structure-property implications for adsorbent design*

SEM-EDS analysis clearly demonstrates that citric acid is a superior binder compared to PVA under one-pot hydrothermal synthesis conditions. Samples synthesized using citric acid (KD-01, KD-06, and KD-07) exhibit enhanced interfacial bonding between AC, zeolite, and magnetite, whereas PVA-based samples (KD-03 and KD-04) show pronounced phase separation. XRD results confirm that the crystalline phases of AC (around 26°) and magnetite (peaks at 30°, 35°, and 43°) are preserved during synthesis. The diminished zeolite diffraction intensity suggests partial structural masking or reduced retention, consistent with elemental analysis. FTIR analysis indicates successful surface modification toward reduced hydrophilicity, as evidenced by weaker hydroxyl-related absorption bands. This property is critical for CO_2 adsorption under realistic flue gas conditions containing moisture. Finally, BET analysis reveals a favorable hierarchical pore structure, combining mesoporous transport channels with microporous adsorption sites. The presence of pores below 20 Å, particularly in KD-06 and KD-07, is a textural feature often associated with enhanced confinement of small gas molecules such as CO_2 (kinetic diameter 3.3 Å). While adsorption measurements are required to confirm this, the observed pore architecture satisfies key textural prerequisites for further evaluation in gas separation applications.

3.2. *Comparison with literature*

To contextualize the textural properties of the synthesized composites, Table 3 presents a comparison with previously reported AC-Z, Z-Fe_3O_4, and related composite materials from the literature. The values for the present work (KD-01 and KD-07) are included for direct comparison. The comparison reveals several important observations. First, the MAGZA composite (zeolite-magnetite) reported by Sani Kovo et al. [29] exhibits a surface area of 110.5 m^2/g and pore volume of 0.185 cm^3/g. In contrast, the AC-Z-Fe_3O_4 composites synthesized in this work (KD-01 and KD-07) demonstrate substantially higher surface areas (450-550 m^2/g) and pore volumes (0.26-0.32 cm^3/g). This enhancement is attributed to the incorporation of high surface area activated carbon, which is absent in the MAGZA system. Second, the pore size distribution of the present composites (2.6-3.1 nm) falls within the range reported for AC-Z hybrids (16-50 nm in Ref. [25]) but skewed toward the micropore/small mesopore region. The smaller pore sizes observed in KD-07 (2.63 nm) compared to KD-01 (3.14 nm) confirm the pore-refining effect of magnetite incorporation noted in Section 3.1.4. Third, compared to pristine Philippine natural zeolite (33.9 m^2/g) and its magnetite-functionalized derivative (45.1 m^2/g) [30], the present composites show order-of-magnitude higher surface areas, highlighting the advantage of combining synthetic zeolite 13X with activated carbon rather than using natural zeolites alone. Fourth, the surface areas achieved in this work approach the lower range of pristine activated carbons (725-1523 m^2/g [31]) while adding the benefits of zeolite microporosity and magnetic functionality. This demonstrates that the citric acid-assisted synthesis successfully preserves much of the activated carbon's porosity while integrating the other components. The textural properties of KD-01 and KD-07 compare favorably with literature values for similar multicomponent systems, confirming that the one-pot hydrothermal method with citric acid binder produces composites with competitive surface areas and well-developed porosity suitable for further evaluation in adsorption applications.

4. Conclusion

AC-Z-Fe_3O_4 composites were successfully synthesized through citric acid-assisted one-pot hydrothermal treatment followed by carbonization. Citric acid proved superior to PVA or binder-free methods, promoting uniform integration of AC, zeolite, and magnetite. SEM-EDS confirmed strong interfacial bonding and homogeneous Fe distribution, while XRD preserved AC and magnetite crystallinity with partial

Table 3
Comparison with previously reported AC-Z-Fe_3O_4.

Material	Composition	BET Surface Area (m^2/g)	Total Pore Volume (cm^3/g)	Average Pore Size (nm)	Application	Reference
Activated carbon-zeolite-magnetite (KD-01)	AC + Zeolite 13X (citric acid)	550	0.32	3.14	Potential CO_2 capture	This work
Activated carbon-zeolite-magnetite (KD-07)	AC + Zeolite 13X + 2g Fe_3O_4 (citric acid)	450	0.26	2.63	Potential CO_2 capture	This work
AC-Z hybrid	Activated carbon/zeolite nanocomposite	Not reported	Not reported	16-50	Drinking water treatment	[25]
MAGZA composite	Zeolite-magnetite	110.5 ± 6	0.185 ± 0.2	6.32 ± 0.8	Heavy metal adsorption	[29]
Zeolite A	Synthetic zeolite A	119.98 ± 3	0.039 ± 0.1	3.33	Reference material	[29]
Magnetite NPs	Fe_3O_4 nanoparticles	95.26 ± 2	0.028 ± 0.1	2.54 ± 0.04	Reference material	[29]
Philippine natural zeolite (MPNZ)	Natural zeolite (modified)	33.88	Not reported	Not reported	Heavy metal removal	[30]
Philippine natural zeolite-magnetite (PNZM)	Natural zeolite + magnetite	45.05	Not reported	Not reported	Heavy metal removal	[30]

retention of the zeolite framework. FTIR analysis indicated decreased surface hydrophilicity, and BET revealed hierarchical micropore-mesopore networks with pore sizes below 20 Å, combining high surface area with effective transport pathways. These results establish the synthesized composites as structurally robust materials with tunable textural properties. The systematic comparison demonstrates that citric acid is superior to PVA for achieving homogeneous phase integration in AC-Z-Fe_3O_4 systems. The resulting composites exhibit hierarchical pore networks combining micro- and mesoporosity, along with reduced surface hydrophilicity compared to pristine zeolite. While this study is limited to synthesis and structural characterization, the findings provide a well defined material platform and establish key structure-property relationships that can inform future investigations into adsorption performance. The incorporation of magnetite additionally offers magnetic functionality for potential ease of material handling.

CRediT authorship contribution statement

Lydia Anggraini: Writing – review & editing, Validation, Supervision, Resources, Project administration, Methodology, Investigation, Funding acquisition, Formal analysis, Conceptualization. **Waqar Hussain:** Writing – review & editing, Writing – original draft, Visualization, Validation, Methodology, Formal analysis, Conceptualization. **Kadek Dharmayudha Aryaputra:** Methodology, Investigation, Conceptualization. **Syed Abdul Moiz Hashmi:** Writing – review & editing. **Serene Lock Sow Mun:** Writing – review & editing, Conceptualization. **Hadiyawarman:** Writing – review & editing. **Mahardika Fahrudin Rois:** Writing – review & editing.

Funding

This research did not receive any specific grant from funding agencies in the public, commercial, or not-for-profit sectors.

Conflict of interest

The authors have declared no conflict of interest.

List of Abbreviations

PVA Polyvinyl alcohol
AC Activated carbon
BET Brunauer-Emmett-Teller
BRIN Badan Riset dan Inovasi Nasional
EDS Energy-dispersive X-ray spectroscopy
SEEI Sustainable Energy & Environmental Innovation
SEM Scanning electron microscopy
XRD X-ray diffraction
FTIR Fourier-transform infrared spectroscopy

Data availability

No data was used for the research described in this article.

References

[1] IPCC, Climate Change, The Physical Science Basis. Contribution of Working Group I to the Sixth Assessment Report of the Intergovernmental Panel on Climate Change, Cambridge University Press., 2021, 2021, https://www.ipcc.ch/report/ar6/wg1/.
[2] Z.H. Lee, K.T. Lee, S. Bhatia, A.R. Mohamed, Post-combustion carbon dioxide capture: evolution towards utilization of nanomaterials, Renew. Sustain. Energy Rev. 16 (2012) 2599–2609, https://doi.org/10.1016/j.rser.2012.01.077.
[3] L. Parker, P. Folger, Capturing CO_2 from coal-fired power plants: challenges for a comprehensive strategy. Coal-Fired Power Plants and Carbon Dioxide Issues, 2011, pp. 1–45.
[4] L. Marques, M. Monteiro, C. Cenci, M. Mateus, J. Condeço, Review of post-combustion carbon capture in Europe: current technologies and future strategies for largest CO_2-Emitting industries, Energies 18 (2025) 1–42, https://doi.org/10.3390/en18133539.
[5] P. Gkotsis, E. Peleka, A. Zouboulis, Membrane-based technologies for post-combustion CO_2 capture from flue gases: recent progress in commonly employed membrane materials, Membranes 13 (2023), https://doi.org/10.3390/membranes13120898.
[6] S. Kundu, T. Khandaker, M.A.A.M. Anik, M.K. Hasan, P.K. Dhar, S.K. Dutta, M. A. Latif, M.S. Hossain, A comprehensive review of enhanced CO_2 capture using activated carbon derived from biomass feedstock, RSC Adv. 14 (2024) 29693–29736, https://doi.org/10.1039/d4ra04537h.
[7] F. Raganati, F. Miccio, P. Ammendola, Adsorption of carbon dioxide for post-combustion capture: a review, Energy Fuels 35 (2021) 12845–12868, https://doi.org/10.1021/acs.energyfuels.1c01618.
[8] A.I. Osman, M. Hefny, M.I.A. Abdel Maksoud, A.M. Elgarahy, D.W. Rooney, Recent Advances in Carbon Capture Storage and Utilisation Technologies: a Review, Springer International Publishing, 2021, https://doi.org/10.1007/s10311-020-01133-3.
[9] H. Zentou, B. Hoque, M.A. Abdalla, A.F. Saber, O.Y. Abdelaziz, M. Aliyu, A. M. Alkhedhair, A.J. Alabduly, M.M. Abdelnaby, Recent advances and challenges in solid sorbents for CO_2 capture, Carbon Capture Sci. Technol. 15 (2025) 100386, https://doi.org/10.1016/j.ccst.2025.100386.
[10] S.A.M. Hashmi, H. Moiz, W. Hussain, M. Mumtaz, Enhanced CO2CH4 separation using hydroxyl functionalized Mg-MOF-74, Chem. Eng. Commun. 212 (2025) 1839–1855, https://doi.org/10.1080/00986445.2025.2503004.
[11] S.A.M. Hashmi, W. Hussain, H. Bhanbhro, H. Rasool, Engineering hierarchical zeolites: mechanistic insights, predictive framework, and deployment pathways, Comments Mod. Chem. (2025) 1–81, https://doi.org/10.1080/02603594.2025.2569055, 00.
[12] S.A.M. Hashmi, M.H. Rasool, W. Hussain, H. Moiz, Activated carbons for direct air capture: adsorption mechanisms, material design and performance optimization, J. Pet. Chem. Eng. 3 (2025) 80–88.
[13] J. Wang, Q. Pu, P. Ning, S. Lu, Activated carbon-based composites for capturing CO_2: a review, Greenh. Gases Sci. Technol. 11 (2021) 377–393, https://doi.org/10.1002/ghg.2051.
[14] S.A. Ganiyu, Review of zeolitic-based sorbents for CO_2 capture: insights into functional modifications, economic feasibility and machine learning-enhanced strategies, Chem. Eng. J. Adv. 23 (2025) 100818, https://doi.org/10.1016/j.ceja.2025.100818.
[15] C.J. Heard, L. Grajciar, F. Uhlík, M. Shamzhy, M. Opanasenko, J. Čejka, P. Nachtigall, Zeolite (in)Stability under aqueous or steaming conditions, Adv. Mater. 32 (2020) 1–29, https://doi.org/10.1002/adma.202003264.

[16] G.S. Yang, The effect of different moisture levels on the toluene desorption rates of modified natural zeolite during MW irradiation, J. Mater. Cycles Waste Manag. 18 (2016) 113–122, https://doi.org/10.1007/s10163-014-0327-x.
[17] M. Mambetova, K. Dossumov, M. Baikhamurova, G. Yergaziyeva, Sorbents based on natural zeolites for carbon dioxide capture and removal of heavy metals from wastewater: current progress and future opportunities, Processes 12 (2024), https://doi.org/10.3390/pr12102071.
[18] D.G. Boer, J. Langerak, P.P. Pescarmona, Zeolites as selective adsorbents for CO_2 separation, ACS Appl. Energy Mater. 6 (2023) 2634–2656, https://doi.org/10.1021/acsaem.2c03605.
[19] X. Liu, C. Wang, C. Chen, Z. Pan, C. Gao, W. Lai, J. Zhao, T. Tian, W. Xiao, Recent advances in hierarchical porous materials for CO_2 capture and utilization, Coord. Chem. Rev. 544 (2025) 216927, https://doi.org/10.1016/j.ccr.2025.216927.
[20] D. Santos-Carballal, A. Roldan, N.Y. Dzade, N.H. de Leeuw, Reactivity of CO_2 on the surfaces of magnetite (Fe3O4), greigite (Fe3S4) and mackinawite (FeS), Philos. Trans. R. Soc. A Math. Phys. Eng. Sci. 376 (2017) 20170065, https://doi.org/10.1098/rsta.2017.0065.
[21] M. Yan, C. Sun, K. Sun, D. Chen, L. Xu, S. Han, X. Li, Advances in magnetic nanocomposite adsorbents for water remediation: design, performance, and challenges, Nanomaterials 15 (2025) 1–24, https://doi.org/10.3390/nano15181425.
[22] V. Phouthavong, R. Yan, S. Nijpanich, T. Hagio, R. Ichino, L. Kong, L. Li, Magnetic adsorbents for wastewater treatment: advancements in their synthesis methods, Materials (Basel) 15 (2022), https://doi.org/10.3390/ma15031053.
[23] A.V. Pastukhov, Magnetic carbonaceous adsorbents derived from nanocomposites of hypercrosslinked polystyrenes, Mater. Today Commun. 39 (2024) 109043, https://doi.org/10.1016/j.mtcomm.2024.109043.
[24] S. Vohl, I. Ban, J. Stergar, M. Slemnik, Synthesis, characterization, and application of magnetic zeolite nanocomposites: a review of current research and future applications, Nanomaterials 15 (2025) 1–33, https://doi.org/10.3390/nano15120921.
[25] A. Kazempour, M.M. Bagheri-Mohagheghi, Activated carbon/zeolite hybrid nanocomposite for drinking water treatment applications: structural, optical, and surface adsorption properties, water, air, Soil Pollut 234 (2023) 669, https://doi.org/10.1007/s11270-023-06676-z.
[26] R. Panek, M. Medykowska, K. Szewczuk-karpisz, Comparison of physicochemical properties of fly ash precursor, Na-P1(C) zeolite–carbon composite and Na-P1 zeolite— adsorption affinity to divalent Pb and Zn cations, Materials (Basel) 1 (2021) 1–20.
[27] T. Zhou, S. Ma, B. Wang, X. Jiang, A promising core–shell carbon-zeolite composite catalyst prepared from distiller's grain pyrolysis residue for enhanced low-temperature NH_3-SCR of NOx, Fuel 411 (2026) 138030, https://doi.org/10.1016/j.fuel.2025.138030.
[28] L. Bandura, R. Panek, J. Madej, W. Franus, Synthesis of zeolite-carbon composites using high-carbon fly ash and their adsorption abilities towards petroleum substances, Fuel 283 (2021), https://doi.org/10.1016/j.fuel.2020.119173.
[29] A.S. Kovo, S. Alaya-Ibrahim, A.S. Abdulkareem, O.D. Adeniyi, T.C. Egbosiuba, J. O. Tijani, M. Saheed, B.O. Okafor, Y.S. Adeyinka, Column adsorption of biological oxygen demand, chemical oxygen demand and total organic carbon from wastewater by magnetite nanoparticles-zeolite A composite, Heliyon 9 (2023) e13095, https://doi.org/10.1016/j.heliyon.2023.e13095.
[30] B.B. Faustino, R.M. Vequizo, R.T. Candidato, Microstructure and adsorption studies on the simultaneous removal of Cu2+, Ni2+, and Zn2+ from simulated wastewater using magnetically functionalized Philippine natural zeolite composite, Open Ceram 24 (2025) 100845, https://doi.org/10.1016/j.oceram.2025.100845.
[31] E. Kacan, Optimum BET surface areas for activated carbon produced from textile sewage sludges and its application as dye removal, J. Environ. Manag. 166 (2016) 116–123, https://doi.org/10.1016/j.jenvman.2015.09.044.